Journal of Computational Mathematics, Vol.15, No.3, 1997, 345–364.

SHOCK INTERACTIONS IN NONEQUILIBRIUM HYPERSONIC FLOW*[1)]

Taehoon Park[2)]
(*Department of Mathematics, The University of North Carolina at Chapel Hill, USA*)
You-lan Zhu
(*Department of Mathematics, The University of North Carolina at Charlotte, USA*)

Abstract

A shock interaction problem is solved with finite difference methods for a hypersonic flow of air with chemical reactions. If a body has two concave corners, a secondary shock is formed in the shock layer and it meets the main shock later. As the two shocks meet, the flow becomes singular at the interaction point, and a new main shock, a contact discontinuity and an expansion wave appear as a result of interaction between the two shocks. Therefore, the problem is very complicated. Using proper combinations of implicit and explicit finite difference schemes according to the property of the equations and the boundary conditions, we compute the flow behind the interaction point successfully.

1. Introduction

In a flow field around a space shuttle, there is more than one shock and there exist interactions between shocks. Noticing this fact, the second author has developed accurate numerical methods for such types of shock interaction problems in three dimensional steady flow [6, 7]. There the gas is assumed to be perfect gas [6] or in equilibrium state [7]. However, in many cases, the nonequilibrium effect has to be considered. Therefore, we would like to generalize our method to nonequilibrium flow. To start with, we consider shock interaction problems in two dimensional nonequilibrium flow.

Suppose a wedge is placed in a hypersonic flow. In this case a shock starting from the edge of the wedge appears if the angle of the wedge is not very large. If the body expands at a later point, a secondary shock forms in the reacting flow region. The slope of the secondary shock is larger and it meets the main shock later. As such two shocks meet, a new shock, a contact discontinuity and an expansion wave generate. Therefore, the flow field is very complicated.

In order to get accurate numerical results, we take all the strong discontinuities (shocks and contact discontinuities) and the weak discontinuities (boundaries of expansion waves) as boundaries. In this case the problem we are going to solve, from the mathematical point of view, is an initial-boundary value problem with several different

* Received May 29, 1995.
1) This work was partially supported by the North Carolina Supercomputing Center.
2) This work is part of this author's Ph.D. Dissertation and partially supported by TGRC-KOSEF.

types of moving boundaries. Since the flow is nonequilibrium, the system of equations possesses stiff source terms. Therefore, in order to solve such a problem, we have to have a method which can be used to different types of initial-boundary value problems with stiff source terms. In this paper, we present such a method. An important feature of the method is to use proper combination of implicit and explicit schemes. Another essential ingredient of our method is an efficient implicit treatment of the right-hand side terms of equations to avoid numerical difficulties arising from stiffness. As has been shown in [2, 3], smooth transformations of domains are successful in overcoming difficulties caused by great gradients of solutions. In this paper, we still keep the coordinate transformation we have used in [3], which has two parameters determining the ratios of physical and computational mesh sizes near the upper and lower boundaries of a domain respectively.

At the beginning, there is only one shock, the numerical method is the same as in [3]. When the body expands at a later point, we need to determine the initial slope of the secondary shock using the jump conditions on shocks and the slope of the body after expansion. In this case there are two shocks in the flow field and a new numerical method is needed. When the secondary shock meets the main shock, we have to solve a Riemann problem to determine the new flow field [5], including the structure of the flow field, the initial slopes of the new shock, the contact discontinuity and the boundaries of the expansion wave and all the physical quantities in the new flow field. In this case, there are five boundaries, including the body surface.

Since our method is suitable to quite general cases, the two types of initial-boundary value problems before and after the meeting of two shocks can be solved by using our method. A computer code based on our method has been written in Fortran for numerical experiments. In the code the mesh size in the marching direction is self-adjusted according to a given error level for an accurate and efficient computation. Using the code, we have obtained accurate details of such a complicated shock interaction problem in two dimensional hypersonic steady reacting flows.

2. System of Equations

The problem we consider is hypersonic flow around bodies with chemical reactions. In our chemical model of air only dissociation-recombination reactions, atom exchange reactions, and bimolecular reactions are considered. Ionization is neglected. Therefore, there are 5 species and 18 reactions. The species are O, N, NO, O_2, N_2, which we call the first, $\cdots$, the fifth species respectively in what follows. 18 reactions considered in the computations are tabulated in Table 1. Also the vibrational excitation of biatomic molecules is assumed half-excited so that its energy content is $RT/2$ [1]. The Euler and chemical equations are strongly coupled. We consider the Euler equations for the steady-state configuration:

$$\boldsymbol{V} \cdot \nabla \rho + \rho \nabla \cdot \boldsymbol{V} = 0, \tag{1}$$

$$(\boldsymbol{V} \cdot \nabla)\, \boldsymbol{V} + \frac{\nabla p}{\rho} = 0, \tag{2}$$

$$\boldsymbol{V} \cdot \left(\nabla h - \frac{\nabla p}{\rho} \right) = 0. \tag{3}$$

Here $\boldsymbol{V}$, ρ, p and h denote the velocity vector, density, pressure and enthalpy respectively. We neglect the diffusion of the species and we write the equations of the production of the species along streamlines:

$$\boldsymbol{V} \cdot \nabla q_i = \omega_i, \quad i = 1, 2, 3. \tag{4}$$

Here, q_i denotes the concentration in unit $g\text{-}mole \cdot g^{-1}$ and the source term ω_i gives the rate of production for the i-th species. The free stream air is considered to be a mixture of 21% oxygen and 79% nitrogen. The mass conservation law provides the concentrations q_4 and q_5 of the fourth species O_2 and the fifth species N_2, respectively:

$$\begin{aligned} q_4 &= \frac{0.21}{\mu} - \frac{q_1 + q_3}{2}, \\ q_5 &= \frac{0.79}{\mu} - \frac{q_2 + q_3}{2}, \end{aligned} \tag{5}$$

where μ is the average molecular weight of air that is 28.8 $g/g\text{-}mole$. The reaction rates ω_i in unit of $g\text{-}mole \cdot g^{-1} \cdot s^{-1}$ and all the formulae and coefficients needed for calculating ω_i can be found in Rakich et al. [4]

Table 1 Reactions considered

i	reaction
1	$O_2 + X \rightleftharpoons O + O + X$
2	$N_2 + X \rightleftharpoons N + N + X$
3	$NO + X \rightleftharpoons N + O + X$
4	$NO + O \rightleftharpoons O_2 + N$
5	$N_2 + O \rightleftharpoons NO + N$
6	$N_2 + O_2 \rightleftharpoons NO + NO$

X means any of the 5 species

With the present assumption, the state equation can be written as [4]

$$p = \rho R T \mathcal{Z} \tag{6}$$

and the expression for h is

$$h = \frac{p}{\rho} \frac{3 + \mathcal{Z}}{\mathcal{Z}} + \sum_{i=1}^{3} h_i^0 q_i, \tag{7}$$

where the compressibility factor $\mathcal{Z}$ is

$$\mathcal{Z} = 1 + \mu \frac{q_1 + q_2}{2} \tag{8}$$

and h_i^0 are the formation energies of the species O, N and NO.

From the expression (7) we know h is a function of p, ρ, q_1, q_2, q_3. Noticing this fact and using the chemical equations (4), the energy equation (3) can be rewritten as

$$\boldsymbol{V} \cdot \nabla \rho = \frac{1}{a^2} \boldsymbol{V} \cdot \nabla p - \Psi. \tag{9}$$

Here, a is the frozen speed of sound:

$$a^2 = \frac{\partial h / \partial \rho}{1/\rho - \partial h / \partial p}, \tag{10}$$

and the term Ψ depends on the rates of production ω_i of species:

$$\Psi = \sum_{i=1}^{3} \omega_i \frac{\partial h / \partial q_i}{\partial h / \partial \rho}. \tag{11}$$

We now derive the equations we will use in our computation. Introduce a $\{z, r\}$-Descartes coordinate system and let

$$\sigma = \frac{v}{u} \quad \text{and} \quad V = \sqrt{u^2 + v^2}, \tag{12}$$

where u and v are the velocity components in the z and r directions respectively. Using equation (9) and taking p, h, σ, q_1, q_2, q_3 as dependent variables, we can have the following form of the Euler and the chemical equations under the $\{z, r\}$-Descartes coordinate system:

$$\left(1 - \frac{a^2}{u^2}\right)p_z + \sigma p_r + \rho a^2 \sigma_r = \frac{a^2}{u}\Psi, \tag{13}$$

$$\sigma_z + \sigma\sigma_r + \frac{p_r - \sigma p_z}{\rho u^2} = 0, \tag{14}$$

$$h_z - \frac{p_z}{\rho} + \sigma\left(h_r - \frac{p_r}{\rho}\right) = 0, \tag{15}$$

$$(q_i)_z + \sigma(q_i)_r = \frac{\omega_i}{u}, \quad i = 1, 2, 3, \tag{16}$$

and this system is completed by the integrated form of the energy equation

$$H = h + \frac{V^2}{2} = \text{constant}. \tag{17}$$

We assume that the equation for the body is $r = b(z)$ and the equation for the main shock is $r = s(z)$ in the $\{z, r\}$-coordinate system and the computational domain is $b(z) \le r \le s(z)$ and $\eta_0^* \le z \le \eta_1^*$. We now introduce a computational frame $\{\eta, \xi\}$:

$$z = \eta \quad (\eta_0^* \le \eta \le \eta_1^*); \qquad r = G(\eta, \xi).$$

Here $G(\eta, \xi)$ always satisfies the conditions $b(\eta) = G(\eta, 0)$ and $s(\eta) = G(\eta, 1)$ so that $\xi = 0$ at the body and $\xi = 1$ at the shock and the computational domain under the $\{\eta, \xi\}$-coordinate system is rectangular. If a curve $r = f(z)$ wants to be considered as an internal boundary, we will choose such a function $G(\eta, \xi)$ that $f(\eta) = G(\eta, \xi^*)$ for a constant ξ^*. In this way, every boundary will be a straight line in the $\{\eta, \xi\}$-coordinate system, which makes treatment of boundaries easy. In Section 6, some details about $G(\eta, \xi)$ are given. When $G(\eta, \xi)$ is given, we can get the system we need under the $\{\eta, \xi\}$-coordinate system[3]. We assume the flow to be supersonic, i.e., the system to be hyperbolic. In this case, the equations under the $\{\eta, \xi\}$-coordinate system can be rewritten in the following characteristic form:

$$\boldsymbol{G}_j^* \boldsymbol{U}_\eta + \lambda_j \boldsymbol{G}_j^* \boldsymbol{U}_\xi = f_j, \quad j = 1, \cdots, 6. \tag{18}$$

Here, $\boldsymbol{U} = (p, h, \sigma, q_1, q_2, q_3)^*$ and $\boldsymbol{G}_j^*$ is the j-th line of the matrix

$$\boldsymbol{G} = \begin{pmatrix} 1 & 0 & -\rho u^2/\beta & 0 & 0 & 0 \\ -1/\rho & 1 & 0 & 0 & 0 & 0 \\ 1 & 0 & \rho u^2/\beta & 0 & 0 & 0 \\ 0 & 0 & 0 & 1 & 0 & 0 \\ 0 & 0 & 0 & 0 & 1 & 0 \\ 0 & 0 & 0 & 0 & 0 & 1 \end{pmatrix}, \tag{19}$$

where

$$\beta = \sqrt{(u^2 + v^2)/a^2 - 1}. \tag{20}$$

The slopes λ_j of the characteristic curves, along which the signals are convected and which are referred as eigenvalues in the next few sections, are defined as

$$\begin{pmatrix} \lambda_1 \\ \lambda_2 \\ \lambda_3 \\ \lambda_4 \\ \lambda_5 \\ \lambda_6 \end{pmatrix} = \begin{pmatrix} \xi_z + \xi_r(u^2\sigma - a^2\beta)/(u^2 - a^2) \\ \xi_z + \xi_r\sigma \\ \xi_z + \xi_r(u^2\sigma + a^2\beta)/(u^2 - a^2) \\ \xi_z + \xi_r\sigma \\ \xi_z + \xi_r\sigma \\ \xi_z + \xi_r\sigma \end{pmatrix}. \tag{21}$$

The source term f_j, related to the chemical kinetics, is the j-th component of the vector

$$\boldsymbol{f} = \begin{pmatrix} \Psi a^2 u(\beta - \sigma)/[\beta(u^2 - a^2)] \\ 0 \\ \Psi a^2 u(\beta + \sigma)/[\beta(u^2 - a^2)] \\ \omega_1/u \\ \omega_2/u \\ \omega_3/u \end{pmatrix}. \tag{22}$$

If each line $\eta = constant$ is a space-like curve, we can obtain solutions to this system using the marching-technique along the η-direction[6].

3. Boundary Conditions

When the discontinuities are taken as internal boundaries, the solution of flow parameters in the supersonic region is reduced to the solution of initial-boundary-value problems of first order quasi-linear hyperbolic systems with several moving internal boundaries. In this section, we will describe concrete expressions of the boundary and internal boundary conditions which we need for our computation.

We have a natural boundary condition at the body :

$$V_n = 0, \tag{23}$$

where $V_n = \boldsymbol{V} \cdot \boldsymbol{n}$, $\boldsymbol{n}$ being the unit normal vector to the body.

Since the rate of chemical reactions is finite, the shock conditions are similar to those for perfect gas flow. The quantities of flow parameters should satisfy the R-H (Rankine-Hugoniot) conditions

$$\begin{aligned} &\rho_2 V_{n,2} = \rho_1 V_{n,1}, \\ &p_2 + \rho_2 V_{n,2}^2 = p_1 + \rho_1 V_{n,1}^2, \\ &h_2 + \frac{V_{n,2}^2}{2} = h_1 + \frac{V_{n,1}^2}{2} \end{aligned} \tag{24}$$

and

$$q_{i,2} = q_{i,1} \quad i = 1, 2, 3, \tag{25}$$

where $\boldsymbol{n}$ is the unit normal vector to the shock and $V_n = \boldsymbol{V} \cdot \boldsymbol{n}$. A quantity with index 1 denotes a quantity in front of the shock and index 2 means behind the shock. On the main shock the enthalpy h can be expressed as

$$h = \frac{\gamma p}{(\gamma - 1)\rho}. \tag{26}$$

In our model, the molecular vibrations are assumed to be half excited [1] behind the main shock and not excited in front of the main shock. Hence, the ratio of specific heats γ changes across the shock. In front of the main shock $\gamma_1 = 7/5$ and behind the main shock $\gamma_2 = 4/3$. From the R-H conditions, we know that the shock pressure ratio at the main shock in this case should be

$$\frac{p_2}{p_1} = \left(\frac{1}{1+\gamma_2}\right)\left\{\left(1+\gamma_1 M_{n,1}^2\right) + \sqrt{\gamma_2^2 + \gamma_1 M_{n,1}^2\left[\gamma_1 M_{n,1}^2 - 2\left(\frac{\gamma_2^2 - \gamma_1}{\gamma_1 - 1}\right)\right]}\right\}, \tag{27}$$

where $M_{n,1}^2 = V_{n,1}^2/(\gamma_1 p_1/\rho_1)$.

The conditions (24) and (25) also hold for the secondary shock. However, the enthalpy h is given by (7) which is different from the formula (26). Since chemical reactions are frozen across the shock, $\mathcal{Z}$ and $\sum_{i=1}^{3} h_i^0 q_i$ are the same on both sides of the shock. Therefore, the third equation of (24) becomes

$$\frac{3+\mathcal{Z}}{\mathcal{Z}}\frac{p_2}{\rho_2} + \frac{V_{n,2}^2}{2} = \frac{3+\mathcal{Z}}{\mathcal{Z}}\frac{p_1}{\rho_1} + \frac{V_{n,1}^2}{2}. \tag{28}$$

Let $\gamma = (3 + \mathcal{Z})/3$, then $(3 + \mathcal{Z})/\mathcal{Z} = \gamma/(\gamma - 1)$. Therefore, the formula for p_2/p_1 in this case is as usual, i.e.,

$$\frac{p_2}{p_1} = 1 + \frac{2\gamma(M_{n,1}^2 - 1)}{\gamma + 1}. \tag{29}$$

From the first two equations in (24) we can have

$$\frac{\rho_1}{\rho_2} = \frac{1 + \gamma M_{n,1}^2 - p_2/p_1}{\gamma M_{n,1}^2} \tag{30}$$

and

$$\boldsymbol{V}_2 = \boldsymbol{V}_1 - V_{n,1}\left(1 - \frac{\rho_1}{\rho_2}\right)\boldsymbol{n}. \tag{31}$$

The two relations are true for both cases since the expression of h is not used during the derivation.

A contact discontinuity is an internal boundary which the flow does not pass through. The pressures on both sides should be the same although other quantities may be different. The jump conditions at contact discontinuities are as follows:

$$\begin{aligned} p_2 &= p_1, \\ V_{n,1} &= 0, \\ V_{n,2} &= 0, \end{aligned} \tag{32}$$

where $V_n = \boldsymbol{V} \cdot \boldsymbol{n}$, $\boldsymbol{n}$ being the unit normal vector to the contact discontinuity and p_1, $V_{n,1}$ denote p, V_n on one side of the contact discontinuity and p_2, $V_{n,2}$ denote p, V_n on the other side.

By definition of a wave-characteristic surface, the speed normal to the wave-characteristic surface is equal to the speed of sound:

$$|V_n| = a. \tag{33}$$

The condition can be used to determine the slopes of the boundaries of the expansion wave.

3. Numerical Schemes

We will formulate implicit and explicit finite difference schemes in this section. The system of equations under consideration is integrated according to the space-marching technique along the coordinate η[3]. Here we give some two-step second-order schemes which can be used in the space-marching procedure. Since we are dealing with the Euler equations and chemical equations fully coupled, there exist possible numerical difficulties associated with the stiffness. To overcome the difficulty caused by the stiffness, we deal with the right-hand side terms implicitly. We have two basic finite difference schemes, one is explicit and the other implicit. They will be combined in some way depending on the values of these eigenvalues λ_i in a subdomain, especially their values at the two boundaries of a subdomain.

We shall use the following symbols in describing the finite difference schemes:

$$\begin{aligned}
&\Delta_+ \boldsymbol{U}_m = \boldsymbol{U}_{m+1} - \boldsymbol{U}_m,\\
&\Delta_- \boldsymbol{U}_m = \boldsymbol{U}_m - \boldsymbol{U}_{m-1},\\
&\Delta \boldsymbol{U}_m = \boldsymbol{U}_{m+\frac{1}{2}} - \boldsymbol{U}_{m-\frac{1}{2}},\\
&\Delta_\lambda \boldsymbol{U}_m = \begin{cases} \Delta_+ \boldsymbol{U}_m, & \text{for } \lambda < 0\\ \Delta_- \boldsymbol{U}_m, & \text{for } \lambda > 0, \end{cases}\\
&\mu f_m = \frac{1}{2}(f_{m+\frac{1}{2}} + f_{m-\frac{1}{2}}).
\end{aligned}$$

If we omit the subscript j in (18), each equation there is of the form:

$$\boldsymbol{G}^* \frac{\partial \boldsymbol{U}}{\partial \eta} + \lambda \boldsymbol{G}^* \frac{\partial \boldsymbol{U}}{\partial \xi} = f, \tag{34}$$

where $\boldsymbol{U} = (p, h, \sigma, q_1, q_2, q_3)^*$.

At the first step, (34) is approximated by

$$\boldsymbol{G}_m^{*k} \boldsymbol{U}_m^{k+\frac{1}{2}} = \boldsymbol{G}_m^{*k} \boldsymbol{U}_m^k - \frac{1}{2} \lambda_m^k \frac{\Delta \eta}{\Delta \xi} \boldsymbol{G}_m^{*k} \Delta_\lambda \boldsymbol{U}_m^k + \frac{1}{2} \Delta \eta f_m^{k+\frac{1}{2}}. \tag{35}$$

The right-hand side of equation (34) is approximated implicitly to overcome the difficulties arising from stiffness. The implicit term is then approximated by

$$f_m^{k+\frac{1}{2}} \approx f_m^k + Df_m^k (\boldsymbol{U}_m^{k+\frac{1}{2}} - \boldsymbol{U}_m^k), \tag{36}$$

where Df is the gradient of f and our scheme becomes

$$\boldsymbol{G}_m^{*k} \boldsymbol{U}_m^{k+\frac{1}{2}} - \frac{1}{2} \Delta \eta Df(\boldsymbol{U}_m^k) \boldsymbol{U}_m^{k+\frac{1}{2}} = \boldsymbol{G}_m^{*k} \boldsymbol{U}_m^k - \frac{1}{2} \frac{\Delta \eta}{\Delta \xi} \lambda_m^k \boldsymbol{G}_m^{*k} \Delta_\lambda \boldsymbol{U}_m^k$$

$$+\frac{1}{2}\Delta\eta f_m^k - \frac{1}{2}\Delta\eta Df(\boldsymbol{U}_m^k)\boldsymbol{U}_m^k. \tag{37}$$

For the second step, (34) is written as

$$\boldsymbol{G}^*\left(\frac{\partial \boldsymbol{U}}{\partial\eta} \mp \frac{\Delta\xi}{\Delta\eta}\frac{\partial \boldsymbol{U}}{\partial\xi}\right) + \left(\lambda \pm \frac{\Delta\xi}{\Delta\eta}\right)\boldsymbol{G}^*\frac{\partial \boldsymbol{U}}{\partial\xi} = f. \tag{38}$$

Here, if $\lambda > 0$, then the upper signs are chosen; if $\lambda < 0$, then the lower signs are taken. Noticing

$$\frac{\boldsymbol{U}_m^{k+1} - \boldsymbol{U}_{m\pm1}^k}{\Delta\eta} = \left(\frac{\partial \boldsymbol{U}}{\partial\eta} \mp \frac{\Delta\xi}{\Delta\eta}\frac{\partial \boldsymbol{U}}{\partial\xi}\right)_{m\pm\frac{1}{2}}^{k+\frac{1}{2}} + O(\eta^2) + O(\xi^2), \tag{39}$$

we then can have the following second order approximation to (38):

$$\mu\boldsymbol{G}_{m\pm\frac{1}{2}}^{*k+\frac{1}{2}}\frac{\boldsymbol{U}_m^{k+1} - \boldsymbol{U}_{m\pm1}^k}{\Delta\eta} + \left(\mu\lambda_{m\pm\frac{1}{2}}^{k+\frac{1}{2}} \pm \frac{\Delta\xi}{\Delta\eta}\right)\mu\boldsymbol{G}_{m\pm\frac{1}{2}}^{*k+\frac{1}{2}}\frac{\Delta\boldsymbol{U}_{m\pm\frac{1}{2}}^{k+\frac{1}{2}}}{\Delta\xi} = \frac{1}{2}\left(f_m^{k+1} + f_{m\pm1}^k\right), \tag{40}$$

which could be written as

$$\begin{aligned}\mu\boldsymbol{G}_{m\pm\frac{1}{2}}^{*k+\frac{1}{2}}\boldsymbol{U}_m^{k+1} =& \mu\boldsymbol{G}_{m\pm\frac{1}{2}}^{*k+\frac{1}{2}}\boldsymbol{U}_{m\pm1}^k - \left(\frac{\Delta\eta}{\Delta\xi}\mu\lambda_{m\pm\frac{1}{2}}^{k+\frac{1}{2}} \pm 1\right)\mu\boldsymbol{G}_{m\pm\frac{1}{2}}^{*k+\frac{1}{2}}\Delta_\pm\boldsymbol{U}_m^{k+\frac{1}{2}} \\ &+ \frac{1}{2}\Delta\eta\left(f_m^{k+1} + f_{m\pm1}^k\right).\end{aligned} \tag{41}$$

With the approximation

$$f_m^{k+1} \approx f_m^k + Df_m^{k+\frac{1}{2}}(\boldsymbol{U}_m^{k+1} - \boldsymbol{U}_m^k), \tag{42}$$

the scheme becomes

$$\begin{aligned}\left(\mu\boldsymbol{G}_{m\pm\frac{1}{2}}^{*k+\frac{1}{2}} - \frac{1}{2}\Delta\eta Df(\boldsymbol{U}_m^{k+\frac{1}{2}})\right)\boldsymbol{U}_m^{k+1} =& \mu\boldsymbol{G}_{m\pm\frac{1}{2}}^{*k+\frac{1}{2}}\boldsymbol{U}_{m\pm1}^k \\ &- \left(\frac{\Delta\eta}{\Delta\xi}\mu\lambda_{m\pm\frac{1}{2}}^{k+\frac{1}{2}} \pm 1\right)\mu\boldsymbol{G}_{m\pm\frac{1}{2}}^{*k+\frac{1}{2}}\Delta_\pm\boldsymbol{U}_m^{k+\frac{1}{2}} \\ &+ \Delta\eta\mu f_{m\pm\frac{1}{2}}^k - \frac{1}{2}\Delta\eta Df(\boldsymbol{U}_m^{k+\frac{1}{2}})\boldsymbol{U}_m^k.\end{aligned} \tag{43}$$

The above scheme cannot be applied at the boundary points because it requires data from the points outside the local computational region. At the boundary points, we need one-sided schemes. If at the second step, the following approximation is used:

$$\begin{aligned}\mu\boldsymbol{G}_{m\mp\frac{1}{2}}^{*k+\frac{1}{2}}\boldsymbol{U}_m^{k+1} =& \mu\boldsymbol{G}_{m\mp\frac{1}{2}}^{*k+\frac{1}{2}}\boldsymbol{U}_{m\mp1}^k \\ &- \left(\frac{\Delta\eta}{\Delta\xi}\mu\lambda_{m\mp\frac{1}{2}}^{k+\frac{1}{2}} \mp 1\right)\mu\boldsymbol{G}_{m\mp\frac{1}{2}}^{*k+\frac{1}{2}}\Delta_\mp\boldsymbol{U}_m^{k+\frac{1}{2}} \\ &+ \frac{1}{2}\Delta\eta\left(f_m^{k+1} + f_{m\mp1}^k\right),\end{aligned}$$

where the upper signs are chosen in the case $\lambda > 0$ and the lower signs are taken in the case $\lambda < 0$, then it is one-sided scheme. Using the approximation (42), we can further modify it into

$$\begin{aligned}\left(\mu \boldsymbol{G}^{*k+\frac{1}{2}}_{m\mp\frac{1}{2}} - \frac{1}{2}\Delta\eta Df(\boldsymbol{U}^{k+\frac{1}{2}}_m)\right)\boldsymbol{U}^{k+1}_m =& \mu \boldsymbol{G}^{*k+\frac{1}{2}}_{m\mp\frac{1}{2}}\boldsymbol{U}^k_{m\mp1} \\ &- \left(\frac{\Delta\eta}{\Delta\xi}\mu\lambda^{k+\frac{1}{2}}_{m\mp\frac{1}{2}} \mp 1\right)\mu \boldsymbol{G}^{*k+\frac{1}{2}}_{m\mp\frac{1}{2}}\Delta_{\mp}\boldsymbol{U}^{k+\frac{1}{2}}_m \\ &+ \Delta\eta\mu f^k_{m\mp\frac{1}{2}} - \frac{1}{2}\Delta\eta Df(\boldsymbol{U}^{k+\frac{1}{2}}_m)\boldsymbol{U}^k_m.\end{aligned} \tag{44}$$

Using one of these two versions, each equation in (18) can be discretized at every grid point.

It is clear that each equation of (18) can also be written as

$$\boldsymbol{A}^*\frac{\partial \boldsymbol{U}}{\partial\eta} + \boldsymbol{B}^*\frac{\partial \boldsymbol{U}}{\partial\xi} = f, \tag{45}$$

where $\boldsymbol{A} = \boldsymbol{G}_j$ and $\boldsymbol{B} = \lambda_j \boldsymbol{G}_j$. In what follows, we write down an implicit scheme for this equation. At the first step, the equation is discretized by

$$\mu\boldsymbol{A}^{*k}_{m+\frac{1}{2}}\mu\boldsymbol{U}^{k+\frac{1}{2}}_{m+\frac{1}{2}} + \frac{1}{2}\frac{\Delta\eta}{\Delta\xi}\mu\boldsymbol{B}^{*k}_{m+\frac{1}{2}}\Delta\boldsymbol{U}^{k+\frac{1}{2}}_{m+\frac{1}{2}} = \mu\boldsymbol{A}^{*k}_{m+\frac{1}{2}}\mu\boldsymbol{U}^k_{m+\frac{1}{2}} + \frac{1}{2}\Delta\eta\mu f^{k+\frac{1}{2}}_{m+\frac{1}{2}}, \tag{46}$$

and using the approximation (36) at $m + \dfrac{1}{2}$ we obtain

$$\begin{aligned}\mu\boldsymbol{A}^{*k}_{m+\frac{1}{2}}\mu\boldsymbol{U}^{k+\frac{1}{2}}_{m+\frac{1}{2}} + \frac{1}{2}\frac{\Delta\eta}{\Delta\xi}\mu\boldsymbol{B}^{*k}_{m+\frac{1}{2}}\Delta\boldsymbol{U}^{k+\frac{1}{2}}_{m+\frac{1}{2}} - \frac{1}{2}\Delta\eta\mu\left[Df^k_{m+\frac{1}{2}}\boldsymbol{U}^{k+\frac{1}{2}}_{m+\frac{1}{2}}\right] \\ = \mu\boldsymbol{A}^{*k}_{m+\frac{1}{2}}\mu\boldsymbol{U}^k_{m+\frac{1}{2}} + \frac{1}{2}\Delta\eta\mu f^k_{m+\frac{1}{2}} - \frac{1}{2}\Delta\eta\mu\left[Df^k_{m+\frac{1}{2}}\boldsymbol{U}^k_{m+\frac{1}{2}}\right],\end{aligned} \tag{47}$$

or when grouped in m,

$$\begin{aligned}\frac{1}{2}\Big(\mu\boldsymbol{A}^{*k}_{m+\frac{1}{2}} + \frac{\Delta\eta}{\Delta\xi}\mu\boldsymbol{B}^{*k}_{m+\frac{1}{2}} - \frac{1}{2}\Delta\eta Df^k_{m+1}\Big)\boldsymbol{U}^{k+\frac{1}{2}}_{m+1} \\ + \frac{1}{2}\left(\mu\boldsymbol{A}^{*k}_{m+\frac{1}{2}} - \frac{\Delta\eta}{\Delta\xi}\mu\boldsymbol{B}^{*k}_{m+\frac{1}{2}} - \frac{1}{2}\Delta\eta Df^k_m\right)\boldsymbol{U}^{k+\frac{1}{2}}_m \\ = \mu\boldsymbol{A}^{*k}_{m+\frac{1}{2}}\mu\boldsymbol{U}^k_{m+\frac{1}{2}} + \frac{1}{2}\Delta\eta\mu f^k_{m+\frac{1}{2}} - \frac{1}{2}\Delta\eta\mu\left[Df^k_{m+\frac{1}{2}}\boldsymbol{U}^k_{m+\frac{1}{2}}\right].\end{aligned} \tag{48}$$

For the second step, the equation is first approximated by

$$\begin{aligned}\mu\boldsymbol{A}^{*k+\frac{1}{2}}_{m+\frac{1}{2}}\mu\boldsymbol{U}^{k+1}_{m+\frac{1}{2}} + \frac{1}{2}\frac{\Delta\eta}{\Delta\xi}\mu\boldsymbol{B}^{*k+\frac{1}{2}}_{m+\frac{1}{2}}\Delta\boldsymbol{U}^{k+1}_{m+\frac{1}{2}} \\ = \mu\boldsymbol{A}^{*k+\frac{1}{2}}_{m+\frac{1}{2}}\mu\boldsymbol{U}^k_{m+\frac{1}{2}} - \frac{1}{2}\frac{\Delta\eta}{\Delta\xi}\mu\boldsymbol{B}^{*k+\frac{1}{2}}_{m+\frac{1}{2}}\Delta\boldsymbol{U}^k_{m+\frac{1}{2}} + \frac{1}{2}\Delta\eta\left[\mu f^k_{m+\frac{1}{2}} + \mu f^{k+1}_{m+\frac{1}{2}}\right],\end{aligned} \tag{49}$$

and using the approximation (42) at $m+\frac{1}{2}$, we then obtain our scheme

$$\mu \boldsymbol{A}^{*k+\frac{1}{2}}_{m+\frac{1}{2}} \mu \boldsymbol{U}^{k+1}_{m+\frac{1}{2}} + \frac{1}{2}\frac{\Delta\eta}{\Delta\xi}\mu \boldsymbol{B}^{*k+\frac{1}{2}}_{m+\frac{1}{2}} \Delta \boldsymbol{U}^{k+1}_{m+\frac{1}{2}} - \frac{1}{2}\Delta\eta\mu\left[Df^{k+\frac{1}{2}}_{m+\frac{1}{2}} \boldsymbol{U}^{k+1}_{m+\frac{1}{2}}\right]$$
$$= \mu \boldsymbol{A}^{*k+\frac{1}{2}}_{m+\frac{1}{2}} \mu \boldsymbol{U}^{k}_{m+\frac{1}{2}} - \frac{1}{2}\frac{\Delta\eta}{\Delta\xi}\mu \boldsymbol{B}^{*k+\frac{1}{2}}_{m+\frac{1}{2}} \Delta \boldsymbol{U}^{k}_{m+\frac{1}{2}}$$
$$+ \Delta\eta\mu f^{k}_{m+\frac{1}{2}} - \frac{1}{2}\Delta\eta\mu\left[Df^{k+\frac{1}{2}}_{m+\frac{1}{2}} \boldsymbol{U}^{k}_{m+\frac{1}{2}}\right]. \tag{50}$$

When grouped in m the scheme becomes,

$$\frac{1}{2}\Big(\mu \boldsymbol{A}^{*k+\frac{1}{2}}_{m+\frac{1}{2}} + \frac{\Delta\eta}{\Delta\xi}\mu \boldsymbol{B}^{*k+\frac{1}{2}}_{m+\frac{1}{2}} - \frac{1}{2}\Delta\eta D f^{k+\frac{1}{2}}_{m+1}\Big)\boldsymbol{U}^{k+1}_{m+1}$$
$$+ \frac{1}{2}\Big(\mu \boldsymbol{A}^{*k+\frac{1}{2}}_{m+\frac{1}{2}} - \frac{\Delta\eta}{\Delta\xi}\mu \boldsymbol{B}^{*k+\frac{1}{2}}_{m+\frac{1}{2}} - \frac{1}{2}\Delta\eta D f^{k+\frac{1}{2}}_{m}\Big)\boldsymbol{U}^{k+1}_{m}$$
$$= \mu \boldsymbol{A}^{*k+\frac{1}{2}}_{m+\frac{1}{2}} \mu \boldsymbol{U}^{k}_{m+\frac{1}{2}} - \frac{1}{2}\frac{\Delta\eta}{\Delta\xi}\mu \boldsymbol{B}^{*k+\frac{1}{2}}_{m+\frac{1}{2}} \Delta \boldsymbol{U}^{k}_{m+\frac{1}{2}}$$
$$+ \Delta\eta\mu f^{k}_{m+\frac{1}{2}} - \frac{1}{2}\Delta\eta\mu\Big[Df^{k+\frac{1}{2}}_{m+\frac{1}{2}} \boldsymbol{U}^{k}_{m+\frac{1}{2}}\Big]. \tag{51}$$

This scheme can be used at each mesh. Therefore for each equation in (18), M difference equations can be obtained in a subdomain, M being the number of meshes in the ξ direction in the subdomain.

5. Flow Patterns at the Interaction Point and Expansion Waves

In this section, we will observe flow patterns after interaction of the shocks. Let $r = F_1(z)$ and $r = F_2(z)$ denote the equations of main shock and secondary shock respectively and they meet at the point

$$\begin{cases} r = F_1(z), \\ r = F_2(z). \end{cases} \tag{52}$$

After the interaction point, the flow pattern is shown in Figure 1, i.e., there are a shock on the top, a contact discontinuity in the middle and an expansion wave at the bottom. In order to determine the initial slopes of the shock, the contact discontinuity, the trailing and leading boundaries of the expansion wave, and the flow properties between them, a Riemann problem has to be solved using the flow properties in the single valued Regions 2 and 5. In order to solve a Riemann problem, we have to have jump conditions on shocks and contact discontinuities, and the relations between the flow properties in expansion waves. The jump conditions on shocks and contact discontinuities for our problem can be found in Section 3.

In what follows, we derive the relations on expansion waves for the problem here. Let $\{z_0, r_0\}$ be the coordinates of the interaction point in the $\{z, r\}$-coordinate system and introduce a new polar coordinate system $\{\bar{r}, \theta\}$ centered at that point by

$$\begin{cases} z = \bar{r}\cos\theta + z_0, \\ r = \bar{r}\sin\theta + r_0. \end{cases} \tag{53}$$

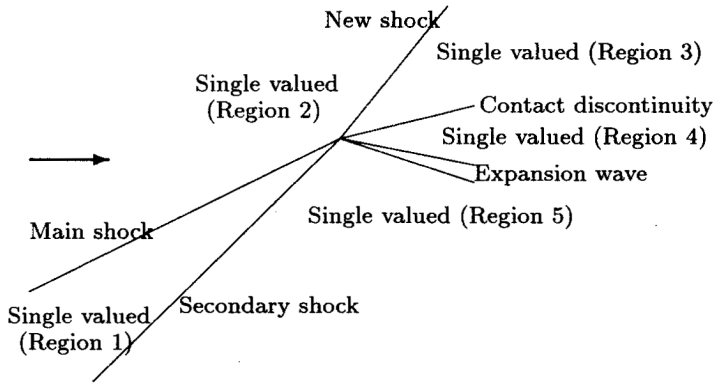

Fig. 1. Flow patterns at the singular point where two shocks interact

From (53) we can easily get the following partial derivatives

$$\begin{pmatrix} \frac{\partial \bar{r}}{\partial z} & \frac{\partial \theta}{\partial z} \\ \frac{\partial \bar{r}}{\partial r} & \frac{\partial \theta}{\partial r} \end{pmatrix} = \begin{pmatrix} \cos\theta & \frac{-\sin\theta}{\bar{r}} \\ \sin\theta & \frac{\cos\theta}{\bar{r}} \end{pmatrix} \tag{54}$$

Since
$$h = h(p, \rho, q_1, q_2, q_3), \tag{55}$$
we have
$$\boldsymbol{V} \cdot \nabla h = \frac{\partial h}{\partial p} \boldsymbol{V} \cdot \nabla p + \frac{\partial h}{\partial \rho} \boldsymbol{V} \cdot \nabla \rho + \frac{\partial h}{\partial q_1} \omega_1 + \frac{\partial h}{\partial q_2} \omega_2 + \frac{\partial h}{\partial q_3} \omega_3 \tag{56}$$

and (3) becomes

$$\boldsymbol{V} \cdot \nabla p - a^2 \boldsymbol{V} \cdot \nabla \rho + \sum_{i=1}^{3} \omega_i \frac{\partial h}{\partial q_i} \Big/ \left(\frac{\partial h}{\partial p} - \frac{1}{\rho} \right) = 0. \tag{57}$$

Therefore, the system (1)–(4) is equivalent to the system which consists of equations (1), (2), (4) and

$$u \frac{\partial p}{\partial z} + v \frac{\partial p}{\partial r} - a^2 u \frac{\partial \rho}{\partial z} - a^2 v \frac{\partial \rho}{\partial r} = -d, \tag{58}$$

where
$$d = \sum_{i=1}^{3} \omega_i \frac{\partial h}{\partial q_i} \Big/ \left(\frac{\partial h}{\partial p} - \frac{1}{\rho} \right). \tag{59}$$

According to (54), the last system can be rewritten into the following system under the $\{\bar{r}, \theta\}$-coordinate system:

$$A_{\bar{r}} \frac{\partial \boldsymbol{W}}{\partial \bar{r}} + \frac{A_\theta}{\bar{r}} \frac{\partial \boldsymbol{W}}{\partial \theta} = D, \tag{60}$$

where

$$A_{\bar{r}} = \begin{pmatrix} V_1 & 0 & \cos\theta/\rho & 0 & 0 & 0 & 0 \\ 0 & V_1 & \sin\theta/\rho & 0 & 0 & 0 & 0 \\ 0 & 0 & V_1 & -a^2 V_1 & 0 & 0 & 0 \\ \rho\cos\theta & \rho\sin\theta & 0 & V_1 & 0 & 0 & 0 \\ 0 & 0 & 0 & 0 & V_1 & 0 & 0 \\ 0 & 0 & 0 & 0 & 0 & V_1 & 0 \\ 0 & 0 & 0 & 0 & 0 & 0 & V_1 \end{pmatrix}, \tag{61}$$

$$A_\theta = \begin{pmatrix} V_2 & 0 & -\sin\theta/\rho & 0 & 0 & 0 & 0 \\ 0 & V_2 & \cos\theta/\rho & 0 & 0 & 0 & 0 \\ 0 & 0 & V_2 & -a^2 V_2 & 0 & 0 & 0 \\ -\rho\sin\theta & \rho\cos\theta & 0 & V_2 & 0 & 0 & 0 \\ 0 & 0 & 0 & 0 & V_2 & 0 & 0 \\ 0 & 0 & 0 & 0 & 0 & V_2 & 0 \\ 0 & 0 & 0 & 0 & 0 & 0 & V_2 \end{pmatrix}, \tag{62}$$

and

$$D = (0, 0, -d, 0, \omega_1, \omega_2, \omega_3)^* ; \boldsymbol{W} = (u, v, p, \rho, q_1, q_2, q_3)^* . \tag{63}$$

Here $V_1 = u\cos\theta + v\sin\theta$, $V_2 = -u\sin\theta + v\cos\theta$. In order to let (60) be true at the interaction point, we require

$$A_\theta \frac{\partial \boldsymbol{W}}{\partial \theta} = 0 \tag{64}$$

at that point. When $V_2 = \mp a$, the determinant of A_θ is equal to zero and there is a nontrivial solution to (64), which satisfies the following equations

$$\begin{aligned} &V_2 \frac{\partial u}{\partial \theta} - \frac{\sin\theta}{\rho}\frac{\partial p}{\partial \theta} = 0, \\ &V_2 \frac{\partial v}{\partial \theta} + \frac{\cos\theta}{\rho}\frac{\partial p}{\partial \theta} = 0, \\ &\frac{\partial p}{\partial \theta} - a^2 \frac{\partial \rho}{\partial \theta} = 0, \\ &\frac{\partial q_i}{\partial \theta} = 0, \quad i = 1, 2, 3, \\ &V_2 = \mp a. \end{aligned} \tag{65}$$

Noticing

$$\begin{aligned} \cos\theta \frac{\partial u}{\partial \theta} + \sin\theta \frac{\partial v}{\partial \theta} &= \frac{\partial V_1}{\partial \theta} - V_2, \\ -\sin\theta \frac{\partial u}{\partial \theta} + \cos\theta \frac{\partial v}{\partial \theta} &= \frac{\partial V_2}{\partial \theta} + V_1, \end{aligned} \tag{66}$$

we can rewrite (65) as

$$\begin{aligned} &\frac{\partial V_1}{\partial \theta} - V_2 = 0, \\ &V_2 \left(\frac{\partial V_2}{\partial \theta} + V_1 \right) + \frac{1}{\rho}\frac{\partial p}{\partial \theta} = 0, \\ &\frac{\partial p}{\partial \theta} - a^2 \frac{\partial \rho}{\partial \theta} = 0, \\ &\frac{\partial q_i}{\partial \theta} = 0, \quad i = 1, 2, 3, \\ &V_2 = \mp a. \end{aligned} \tag{67}$$

From (10) and (7), we know $a^2 = ((3 + \mathcal{Z})/3)\, p/\rho$ or let $\gamma = (3 + \mathcal{Z})/3$, we have $a^2 = \gamma p/\rho$. From (67), we know that q_i dose not depend on θ. Thus γ is independent of

θ. In this case, the system has the following analytic solution

$$\begin{aligned} V_1 &= \sqrt{\bar{H}} \sin\left(\theta\sqrt{\frac{\gamma-1}{\gamma+1}} + \delta\right), \\ V_2 &= \sqrt{\bar{H}\frac{\gamma-1}{\gamma+1}} \cos\left(\theta\sqrt{\frac{\gamma-1}{\gamma+1}} + \delta\right), \\ \rho &= \left(V_2^2 \rho_0^\gamma / \gamma p_0\right)^{\frac{1}{\gamma-1}}, \\ p &= p_0 \left(\rho/\rho_0\right)^\gamma, \\ q_i &= q_{i,0}, \quad i = 1,2,3 \end{aligned} \tag{68}$$

and

$$\begin{aligned} u &= V_1 \cos\theta - V_2 \sin\theta, \\ v &= V_1 \sin\theta + V_2 \cos\theta. \end{aligned} \tag{69}$$

Here the parameters $\bar{H}$, δ, p_0, ρ_0, $q_{1,0}$, $q_{2,0}$, $q_{3,0}$ and γ can be determined by the flow properties in front of the expansion wave, in our case, by the data in Region 5. p_0, ρ_0, $q_{1,0}$, $q_{2,0}$, $q_{3,0}$ denote p, ρ, q_1, q_2, q_3 at the point $\{z_0, r_0\}$ in Region 5. $\bar{H}$, δ and γ can be calculated by the following formulae

$$\begin{aligned} \bar{H} &= V_0^2 + 2\frac{\gamma}{\gamma-1}\frac{p_0}{\rho_0}, \\ \delta &= \sin^{-1}(s) - \sqrt{\frac{\gamma-1}{\gamma+1}} \tan^{-1}\left(\frac{u_0 v_0 - \alpha}{u_0^2 - a_0^2}\right), \\ \gamma &= \frac{3+\mathcal{Z}_0}{3}, \end{aligned} \tag{70}$$

where

$$\begin{aligned} V_0^2 &= u_0^2 + v_0^2, \\ s &= \sqrt{\left(\frac{V_0^2}{\bar{H}} - \frac{\gamma-1}{\gamma+1}\right)\frac{\gamma+1}{2}}, \\ \alpha &= \sqrt{a_0^2\left(u_0^2 + v_0^2 - a_0^2\right)}, \\ a_0^2 &= \frac{3+\mathcal{Z}_0}{3}\frac{p_0}{\rho_0}, \\ \mathcal{Z}_0 &= 1 + \mu\frac{q_{1,0}+q_{2,0}}{2}. \end{aligned} \tag{71}$$

Here u_0, v_0 are u, v at the interaction point in Region 5. Therefore, the flow properties in the expansion wave can be determined by the flow properties in Region 5 and the angle θ.

The Riemann problem can be solved in the following way. First we guess the slope of the contact discontinuity. Then using the relations (24) and (25), we find such a slope of the shock that the flow in Region 3 is parallel to the contact discontinuity. Also

we determine such a θ in the expansion wave that the flow in Region 4 is parallel to the contact discontinuity. Finally we compare the pressure in Region 3 and the pressure in Region 4. If they are equal, we find the solution. If not, we have to adjust the slope of the contact discontinuity. We can use any known method for solving a nonlinear equation to adjust the slope of the contact discontinuity since it actually is a process of solving the equation

$$p_4(F_z) = p_3(F_z), \tag{72}$$

where F_z is the slope of the contact discontinuity and p_3 and p_4 are pressures in Regions 3 and 4 respectively.

6. Numerical Computation of Shock Interaction

We have computed the following shock interaction problem. The free stream conditions are given in Table 2 First, we obtain a main shock by placing a 25 degree wedge in front of the free stream at $z = 0\,m$. Later at $z = 10\,m$, the body expands by 5 degrees. That is, the angle between the body and free streamline changes suddenly from 25 degrees to 30 degrees. At this point a secondary shock is formed. The slope of this shock is much larger and it meets the main shock at $z \approx 13\,m$. As a result of interaction between the two shocks, a new main shock, a contact discontinuity and an expansion wave generate. Therefore, at the beginning there is only one shock. Later there are two shocks. Finally the flow field contains one shock, one contact discontinuity and one expansion wave. In Figure 2 the flow field structure before and after shock interaction is given.

Before $z = 10\,m$, the numerical method given in [3] can be used. At $z = 10\,m$, the jump conditions on shocks (24)–(25) and the boundary condition on bodies (23) are used to determine the initial slope of the secondary shock and all the physical quantities behind it. Now we have two shocks in our computational region and a new method is needed. In this case we take the two shocks and the body as boundaries and $G(\eta, \xi)$ is chosen in such a way that $r = G(\eta, 0.5)$ is the equation for the secondary shock (the details are omitted here). In what follows, the subdomain between the secondary shock and the body is called Zone 1 and the subdomain between the two shocks is referred as Zone 2. In Zone 2, λ_3 is greater than zero at the main shock and it is less than zero at the secondary shock. For any λ with such a feature, it is reasonable for the equation (18) corresponding to this λ to be discretized M_2+1 times, M_2 being the number of meshes in the ξ-direction in Zone 2. Therefore for this equation the explicit scheme is used at all grid points. Since $\lambda_i < 0$ at the two boundaries of Zone 2, $i = 1, 2, 4, 5, 6$, the corresponding equation (18) should be discretized M_2 times. Also the value of these λ_i might be very large. Noticing these

Table 2. Free Stream Conditions

Speed	6.77 Km/s
Altitude	65 Km
Pressure	10.85 N/m^2
Density	1.56×10^{-4} Kg/m^3
Temperature	240.8 $^\circ K$
Mach Number	21.7

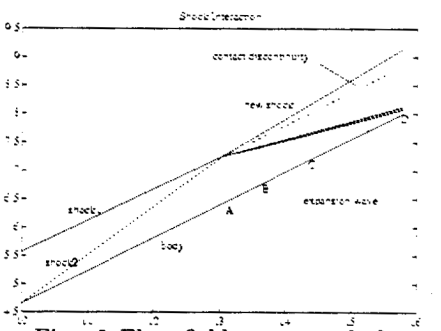

Fig. 2 Flow field structure before and after shock interaction

facts, we adopt the implicit scheme in all the meshes for other equations. Therefore we can get $6M_2 + 1$ equations. Using these difference equations and the jump conditions on the main shock (24)–(25), we can get the solution in Zone 2, including the new slope of the main shock. The pattern of flow field in Zone 1 is similar to that before the secondary shock appears. Therefore, in Zone 1, for all the equations (18) the implicit scheme is used and $6M_1$ equations can be obtained, M_1 being the number of meshes in the ξ-direction in Zone 1. As soon as the solution in front of the secondary shock is obtained, the flow properties in Zone 1, including the slope of the secondary shock, can be gotten by using the $6M_1$ equations and the boundary condition on the body (23) and the jump conditions on the secondary shock (24)–(25). Since the chemical reactions are frozen across the secondary shock, the concentration of species are continuous. Other properties have sudden jumps. None of the flow quantities changes so much within each zone. Therefore, the computation is relatively easy.

When two shocks meet, we take the free stream conditions and the final data behind the secondary shock in Zone 1 as the data for the Riemann problem. After we obtain the solution of the Riemann problem, we can do further computation. We divide our computational region into four zones numbered 1 to 4 from the body to the shock. Zone 1 is between the body and the leading boundary of the expansion wave, Zone 2 is the expansion wave, Zone 3 is between the trailing boundary of the expansion wave and the contact discontinuity, and the region between the new main shock and the contact discontinuity is called Zone 4. In this case, $G(\eta, \xi)$ is so chosen that $r = G(\eta, 0.75)$, $r = G(\eta, 0.5)$ and $r = G(\eta, 0.25)$ are the equations for the contact discontinuity, the trailing boundary and the leading boundary of the expansion wave respectively. In our computation, the function $r = G(\eta, \xi)$ is implicitly defined as follows. Suppose $r = s(\eta) \equiv c_4(\eta)$, $r = c_3(\eta)$, $r = c_2(\eta)$, $r = c_1(\eta)$, $r = b(\eta) \equiv c_0(\eta)$ are the equations for the main shock, the contact discontinuity, the trailing boundary and the leading boundary of the expansion wave and the body respectively. Let $\xi_4 = 1$, $\xi_3 = 0.75$, $\xi_2 = 0.5$, $\xi_1 = 0.25$ and $\xi_0 = 0$. For $r \in [c_{i-1}(\eta), c_i(\eta)]$, let,

$$\xi = \xi_{i-1} + (\xi_i - \xi_{i-1}) \frac{f^{-1}(t) - f^{-1}(\tau_{1,i})}{f^{-1}(\tau_{2,i}) - f^{-1}(\tau_{1,i})}, \quad i = 1, \cdots, 4, \tag{73}$$

where

$$f(t) = \frac{2t}{t^2 + 1}, \tag{74}$$

$$t = \frac{r - c_{i-1}(\eta)}{c_i(\eta) - c_{i-1}(\eta)} (\tau_{2,i} - \tau_{1,i}) + \tau_{1,i}. \tag{75}$$

$\tau_{1,i}$ and $\tau_{2,i}$ are the parameters which determine how small mesh sizes will be used near the boundaries[3] Their values for our computation are

$$\begin{aligned} \tau_{1,1} &= -0.9, & \tau_{2,1} &= 0.9, \\ \tau_{1,2} &= -0.7, & \tau_{2,2} &= 0.7, \\ \tau_{1,3} &= -0.7, & \tau_{2,3} &= 0.7, \\ \tau_{1,4} &= -0.8, & \tau_{2,4} &= 0.8. \end{aligned} \tag{76}$$

In Zone 1, $\lambda_3 > 0$ at the two boundaries, so the equation (18) corresponding to λ_3 should be discretized M_1 times and the implicit scheme is used; In this zone $\lambda_1 = 0$ and

$\lambda_2 = \lambda_4 = \lambda_5 = \lambda_6 > 0$ at the leading boundary of the expansion wave and $\lambda_1 < 0$ and $\lambda_2 = \lambda_4 = \lambda_5 = \lambda_6 = 0$ at the body, so the equations (18) with $j = 1, 2, 4, 5, 6$ should be discretized $M_1 + 1$ times, which can be fulfilled by using the explicit scheme at all the grid points. In this way we can have $6M_1 + 5$ difference equations. Using these equations and the boundary condition on the body (23), we can have the flow properties in this zone. After that, the new slope of the leading boundary of the expansion wave can be obtained by (33). In Zone 2, $\lambda_2, \lambda_3, \lambda_4, \lambda_5, \lambda_6 < 0$ at the two boundaries of this zone, so the corresponding equations (18) need to be discretized M_2 times and the implicit scheme can be used. $\lambda_1 = 0$ at the upper and lower boundaries of this zone and the corresponding equation should be discretized at the trailing boundary of the expansion wave and at all the interior points by the explicit scheme (the equation at the leading boundary of the expansion wave has been used in Zone 1). Therefore $6M_2$ difference equations can be obtained. As soon as the flow properties at the leading boundary of the expansion wave are obtained, the other flow properties in Zone 2 can be determined by using these difference equations. After that, the new slope of the trailing boundary of the expansion wave can be calculated by using (33). In Zone 3, $\lambda_1 < 0$ at the contact discontinuity and the equation (18) with $j = 1$ has been discretized at the trailing boundary of the expansion wave in Zone 2, so the equation should be discretized $M_3 - 1$ times, M_3 being the number of meshes in the ξ-direction in this zone. The value of λ_1 might be very large. Therefore the $M_3 - 1$ times discretization should be done by using the implicit scheme in all the meshes except the mesh next to the trailing boundary of the expansion wave. $\lambda_2, \lambda_3, \lambda_4, \lambda_5, \lambda_6 > 0$ at the trailing boundary of the expansion wave and they are greater than or equal to zero at the contact discontinuity. Thus the corresponding equations should be discretized M_3 times and the implicit scheme should be used because the values of these eigenvalues might be very large. In Zone 4 the situation is similar to the case with only one shock. For each and every λ_i, M_4 difference equations should be obtained, M_4 being the number of meshes in the ξ-direction in this zone, which can be fulfilled by using the implicit scheme. In this way, $6M_3 - 1$ and $6M_4$ difference equations are obtained in Zone 3 and Zone 4 respectively. As long as the solution is given at the trailing boundary of the expansion wave, these difference equations and the jump conditions on the main shock (24)–(25) and the jump conditions on the contact discontinuity (32) provide all the equations needed to determine the other flow properties in Zones 3 and 4, including the new slopes of the main shock and the contact discontinuity. When determining these flow properties, a system consisting of many linear equations and a few nonlinear equations is needed to be solved. This type of system can be efficiently solved by a method called the double-sweeping method[6].

A computer code based on the method described above has been written in Fortran for numerical experiments. In the code the mesh size in the marching direction is self-adjusted according to a given error level for an accurate and efficient computation. Using the code, we have obtained accurate details of such a complicated shock interaction problem. In Fig. 2, the locations of all the boundaries from $z = 10\,m$ to $z = 15.80\,m$ are given.

The flow field after the shock interaction is much more complicated than that before the interaction. Therefore, in this paper we only give some figures about variations of flow properties in the flow field after shock interaction. Variations of flow properties

are given in Figs. 3–12. Each figure has two graphs. In the first graph, the abscissa represents ξ. As we mentioned above, $\xi = 1$, 0.75, 0.5, 0.25 and 0 correspond to the main shock, the contact discontinuity, the trailing boundary and the leading boundary of the expansion wave and the body. In the second picture, the abscissa represents

$$\bar{t} = \frac{r - b(\eta)}{s(\eta) - b(\eta)}. \tag{77}$$

Therefore at the shock and the body the abscissa is still 1 and 0 respectively. The ordinate represents a physical quantity. The unit for each physical quantity can be found in [3]. In each graph, there are four lines labeled A through D. They are the numerical results on the lines marked A through D in Fig. 2; $z = 13.056\,m$ at A, $z = 13.63\,m$ at B, $z = 14.35\,m$ at C and $z = 15.80\,m$ at D. We stopped our computation at D.

All the quantities in Zone 1 are quite smooth because no problems like those behind the shock happen here. Although the width of the expansion wave Zone 2 is very narrow, it is quite strong. Many flow properties change greatly. For example, pressure shows a big decrease across the expansion wave. Though the flow properties are quite smooth in the expansion wave, the weak discontinuity are quite big both on the trailing boundary and the leading boundary of the expansion wave. In Zone 3 the flow properties are also quite smooth. But, at the contact discontinuity the flow properties, except the pressure, have big jumps. In Fig. 5, the jump of density is shown and there is not any smearing. In Zone 4 the flow properties are not as smooth as in other zones. Especially, near the shock, the flow properties vary quite rapidly compared to the flow properties in other zones.

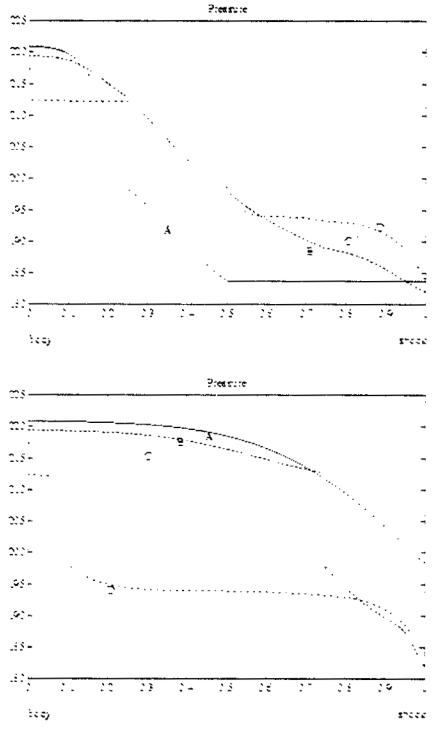

Fig. 3 Pressure after Shock Interaction

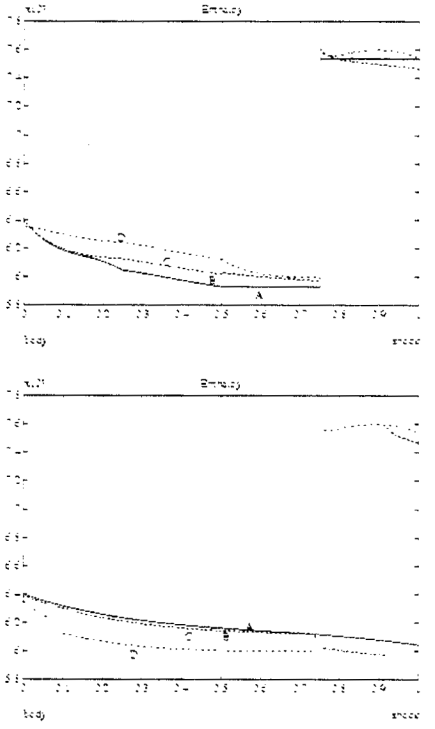

Fig. 4 Enthalpy after Shock Interaction

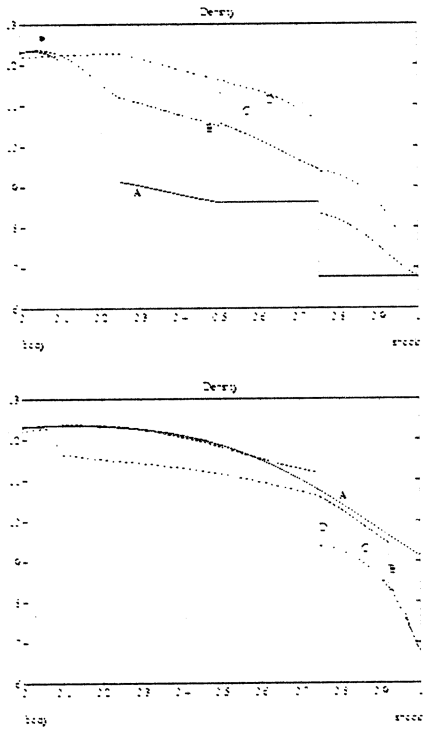

Fig. 5 Density after Shock Interaction

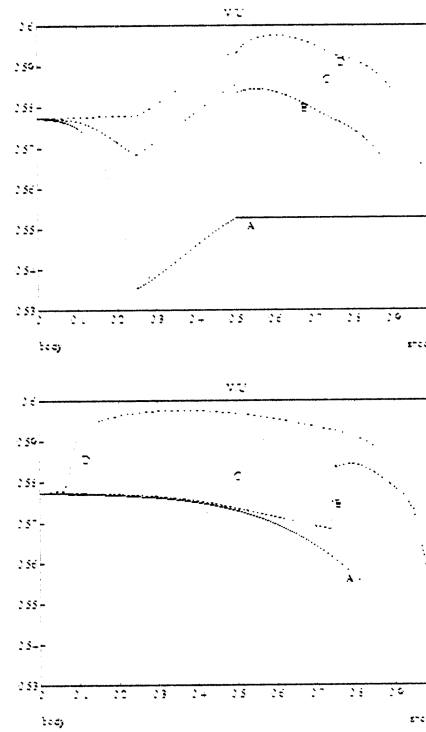

Fig. 6 v/u after Shock Interaction

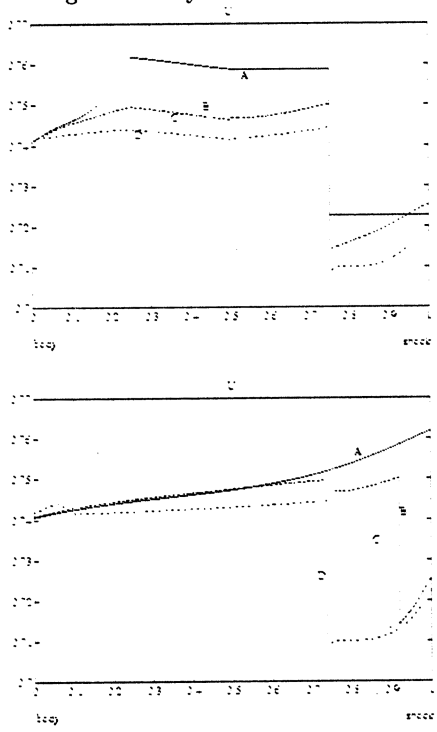

Fig. 7 u after Shock Interaction

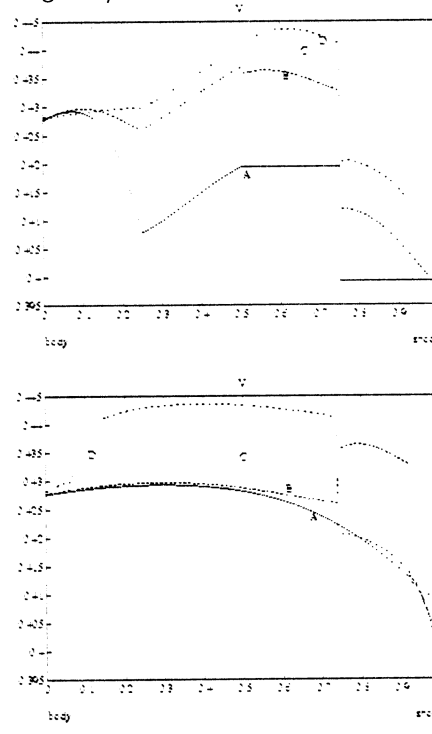

Fig. 8 v after Shock Interaction

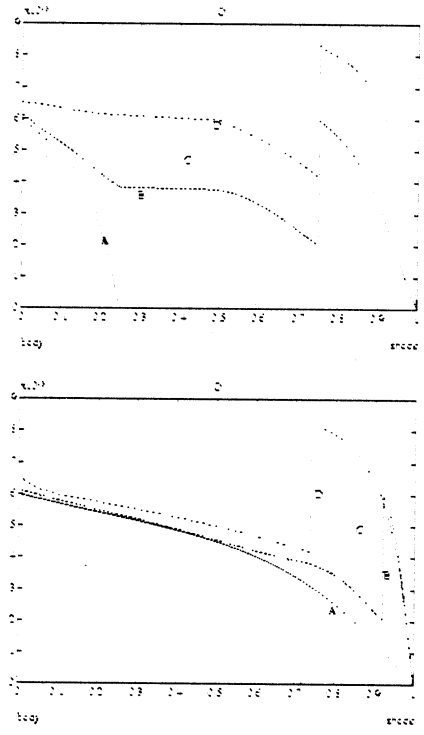

Fig. 9 O after Shock Interaction

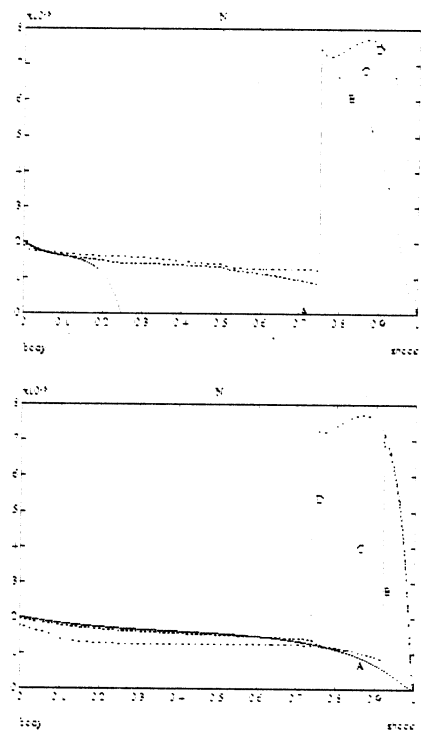

Fig. 10 N after Shock Interaction

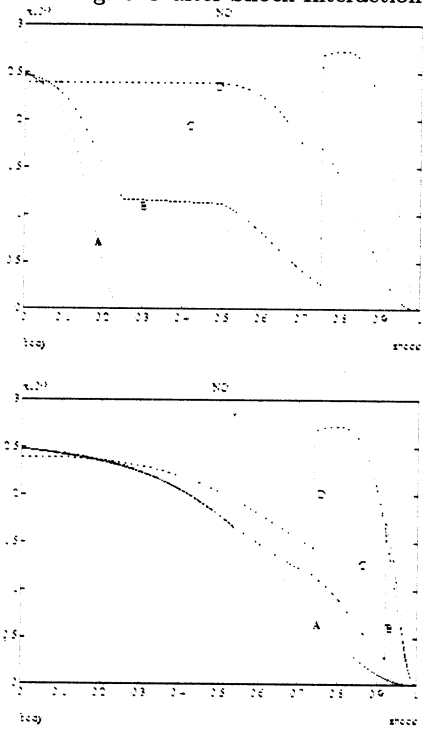

Fig. 11 NO after Shock Interaction

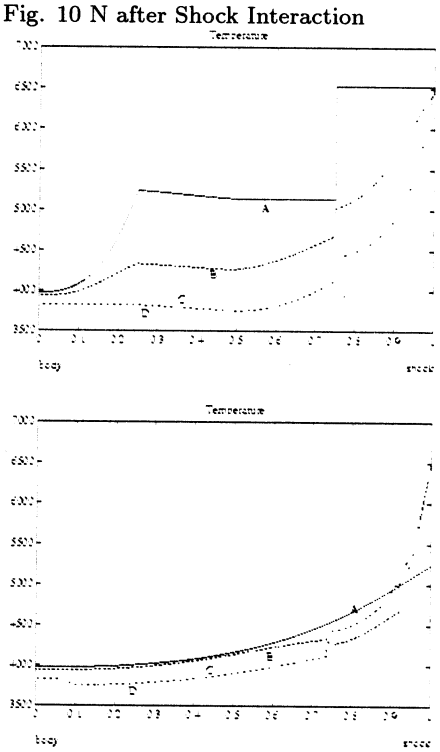

Fig. 12 Temperature after Shock Interaction

In our computational results, the variations of flow properties among the first few grid points in Zone 3 near the trailing boundary of expansion wave are not monotone. This phenomenon might be caused by the difference of numerical schemes used in Zone

2 and in Zone 3. The peaks are not big and become smaller down stream as we can see in Figs 3 and 6. They do not cause any numerical difficulties.

7. Remark

We have quite accurately computed a shock interaction problem in nonequilibrium flow. Since there exist one shock, one contact discontinuity and one expansion wave after shock interaction, the structure of the flow is very complicated. In order to get accurate results, we take the shock, the contact discontinuity and the two boundaries of the expansion wave as computational boundaries. With the body as another boundary, we solve an initial-boundary value problem with 5 boundaries. In each subdomain, the features of boundaries and equations are different. Therefore, for different subdomains, different schemes are usually needed for efficient computation. We present a numerical method, which is suitable to a variety of initial-boundary value problems. With this carefully designed method, we are able to get accurate results for the very complicated shock interaction problem.

Acknowledgements The first author wishes to express his sincere thanks to his advisor Dr. R. Cohen.

References

[1] M.L. Lighthill, Dynamics of dissociating gas, Part I: Equilibrium Flow, *Journal of Fluid Mechanics*, **2**, (1957), 1–32.

[2] T. Park, Computations of Nonequilibrium Hypersonic Inviscid Flow around Bodies, Ph.D. Dissertation, The University of North Carolina at Chapel Hill, 1994.

[3] T. Park and Y.L. Zhu, Computations of Nonequilibrium Hypersonic Flow over Concave Corners, to appear.

[4] J.V. Rakich, H.E. Bailey and C. Park, Computation of nonequilibrium, supersonic three-dimensional inviscid flow over blunt-nosed bodies, *AIAA Journal*, **21** (1983), 834–841.

[5] X.H Wu, Y.L. Zhu and B.M. Chen, A general numerical method for solving riemann problems., *Journal of Computational Math.*, **9** (1991), 369–377.

[6] Y.L. Zhu, X.C. Zhong, B.M. Chen and Z.M. Zhang, Difference Methods for Initial-Boundary-Value Problems and Flow Around Bodies, Springer-Verlag, Heidelberg and Science Press, Beijing, 1988.

[7] Y.L. Zhu, B.M. Chen, X.H. Wu and Q.S. Xu, Some New Development of the Singularity-Separating Difference Method, Lecture Notes in Physics, Springer-Verlag, Heidelberg, Vol. 170, 1982.